



## **DESIGN OF A LOW SPEED RIM-SUPPORTED FAN FOR MINIMUM NOISE**

Mark HURTADO, Ricardo BURDISSO,  
*Virginia Tech, Department of Mechanical Engineering, 445 Goodwin Hall,  
635 Prices Fork Road - MC 0238, Blacksburg, VA 24061, USA*

### **SUMMARY**

Axial flow fans are critical in circulating air in occupied areas, however, they are often loud and cause noise induced hearing loss from prolonged exposure. Consequently, the present paper presents the design of a rim supported fan that eliminates dominant noise sources from commercial fans such as rotor-stator and tip gap noise. Noise sources not eliminated are proportional to the 4-6th power of the fan tip speed, depending on the noise source. Therefore, the rim supported fan has been designed to maximize the flow rate contribution from the blade outer sections to minimize the fan tip speed and noise while preserving the fan flow rate. The fan has been 3D printed and tested showing good agreement with predictions. The performance of the rim mounted fan was compared to the conventional approach of a hub-mounted (free-tip) fan.

### **INTRODUCTION**

Noise induced hearing loss is a concerning byproduct of loud axial fans used to circulate air and control the temperature of occupied areas. Commercial ventilation fans are often loud due poor design features that lead to a poor aerodynamic performance and high noise levels. Some of the major fan noise contributors are the rotor broadband self-noise, rotor-stator tonal interaction, tip gap noise, and blade steady loading and thickness (Padhy, 1994). Rotor-stator and tip gap noise can be eliminated with a rim supported fan design. However, fan noise due to rotor self-noise, blade steady loading and thickness will not be eliminated for a rim supported fan. These noise sources are proportional to the 4-6th power of the fan tip speed, depending on the noise source (Cudina, 1992). Therefore, by minimizing the fan tip speed, the fan noise can be reduced significantly.

To minimize the fan tip speed, the classical free vortex design (FVD) method is often used for the design of axial flow fans. The FVD method is characterized by a constant axial flow velocity and pressure rise along the blade span that maintains the fluid in radial equilibrium. This allows for 2D characteristics of the flow where the swirl velocity is inversely proportional to the radius. One of the disadvantages with the classical FVD method is the high blade root loading that leads to a large twist and chord of the blade section near the hub (Bruneau, 1994). In addition, the FVD limits the contribution of the outside sections of the blade to the performance of the fan. Therefore, to better

design the blade sections at higher radii, the axial velocity need not to be constant along the blade span. An alternative design approach to the classical FVD method is the less conventional controlled vortex design (CVD) approach. The CVD approach is characterized by varying axial velocities along the blade span that maximize the fan performance by better utilizing the blade sections at higher radii (Davis, 1979). As a result, the blade twist and chord at the hub section can be decreased. Therefore, the CVD method allows for the design of high performing fans with a lower speed and smaller fan diameter, i.e. lower tip speed and noise (Vad and Bencze, 1998; Vad and Horvath, 2008). Consequently, the design of a CVD fan is presented in this paper as a promising solution to the increasing need of quiet ventilation fans.

## CONTROL VORTEX DESIGN

The present paper presents a control vortex design (CVD) methodology to design the fan blade profile to minimize fan tip speed and noise while preserving aerodynamic performance. The CVD fan blades are characterized by a span wise changing circulation that ensures a higher flow rate contribution of the blade outer sections, i.e. axial flow increases from the blade hub to the tip. However, a non-uniform span wise circulation is susceptible to radially outward flow that increases near tip losses if the flow is not in radial equilibrium. Consequently, in this study the effect of radial flow is incorporated into the design procedure. To that end, the velocity profile was designed to maintain radial equilibrium and to maximizing the volumetric flow rate. The fan blade sections giving the desired velocity profile constitute the final fan blade design. The design of the blade sections was performed using XROTOR (Drela & Youngren, 2011). This code assumed the fan to be embedded in an infinite long duct of constant annular cross section, e.g. the effects of a duct inlet, outlet, and center body (hub) on the rotor aerodynamics and viscera are not included. To incorporate these effects, the Ducted Fan Design Code (DFDC) was used to design a bell mouth inlet duct to ensure a smooth flow into the fan and to maximize the amount of air drawn with minimum losses, i.e. increase the fan volumetric flow rate (Drela, 2005). Additionally, the tonal and broadband noise of the fan were modeled using the NASA code WOBBLE (Parzych, 1993) and the semi-empirical model developed by (Mugridge and Morfey, 1972) respectively.

### Velocity profile design

Due to the varying axial velocity and pressure across the blade for a CVD approach, designing the blades to maintain radial equilibrium is a significant challenge. The challenge is in designing the blade sections so that the centrifugal force of the rotating fluid is balanced by the radial pressure gradient. If there is no radial equilibrium, there will be a radially outward flow that will increase the tip losses and tip stalling (Vad and Horvath, 2008). Therefore, the velocity profile must be designed to maintain a radial equilibrium along the blade. Radial equilibrium is accomplished when

$$\frac{1}{\rho} \frac{dp_0(r)}{dr} = V_{axial}(r) \frac{dV_{axial}(r)}{dr} + \frac{V_{\theta}(r)}{r} \frac{d(r * V_{\theta}(r))}{dr} \quad (1)$$

where  $\rho$  is the air density,  $V_{\theta}$  is the swirl velocity,  $V_{axial}$  is the axial velocity,  $r$  is the radial position and  $p_0(r)$  is the radial pressure distribution (Dixon and Hall, 2013). The radial pressure distribution can be described using Bernoulli's equation as

$$p_0(r) = p_s(r) + \frac{1}{2} \rho (V_x^2(r) + V_{\theta}^2(r)) \quad (2)$$

where  $p_s(r)$  is the static pressure. Additionally, the swirl velocity can be described using the power law distribution as

$$V_{\theta}(r) = ar^n \quad (3)$$

where  $a$  is the swirl velocity coefficient,  $n$  is the swirl velocity exponent, and  $r$  is the radial position along the blade. It is evident from Equation (3) that when  $n$  is equal to -1, the free vortex swirl velocity given is the assumed profile when using the FVD method. To ensure that a non-uniform flow velocity profile maintains radial equilibrium, the radial equilibrium equation (1) can be solved for the axial velocity distribution along the blade ( $V_{axial}(r)$ ) for a prescribed swirl velocity using Equation (3). The resulting expression gives the velocity distribution that satisfies the radial equilibrium equation. The expression is derived by Louw Et al (Louw et al., 2012) as

$$V_{axial}(r) = \sqrt{2a\Omega(r^{n+1} - r_h^{n+1}) - R(r) * a^2(n+1) + V_{hub}^2} \quad (4)$$

where

$$R(r) = \ln\left(\frac{r}{r_h}\right)^2 \text{ for } n = 0 \quad (5)$$

and

$$R(r) = \frac{r^{2n} - r_h^{2n}}{n} \text{ for } n \neq 0 \quad (6)$$

Therefore, Equation (4) through (6) gives the axial velocity profile that together with the swirl velocity described by equation (3) maintain radial equilibrium. Using a trade study approach, the axial velocity parameters in Equation (4) were investigated to determine the swirl velocity coefficients ( $a$  and  $n$ ), the fan speed ( $\Omega$ ), and the velocity at the hub ( $V_{hub}$ ) that will maximize the volumetric flow rate. As shown in Equation (4) the volumetric flow rate can be increased by setting a higher velocity at the hub. However, the axial velocity at the hub is limited by the angular velocity of the fan. Consequently, to maximize the volumetric flow rate, the maximum velocity at the hub for a given fan speed must be determined. Using the airfoil dimensionless analysis described by Hurtado et al. (Hurtado et al., 2017) the maximum velocity at the hub for a given fan speed can be determined as

$$V_{hub} = \frac{\Omega r_{hub}}{0.6} \quad (7)$$

Using a trade study, the swirl velocity coefficient and  $n$  exponent  $a$  to maximize the volumetric flow rate were found to be 6.202 and -0.092, respectively. Figure 1(a) and (b) show the corresponding axial and swirl velocity profiles for a fan tip Mach number of 0.14 and diameter of 0.362 meters (14.25 inches), respectively. Figure 1 shows that a non-uniform axial velocity profile also results in a lower swirl velocity at the inner radius when compared to a free vortex swirl velocity that is inversely proportional to the radial position. Similar results presented by Von Backstrom et al. (Von Backstrom et al., 1996) show that the non-uniform axial velocity profile results in a decrease of exit dynamic losses as shown in Figure 1(b).

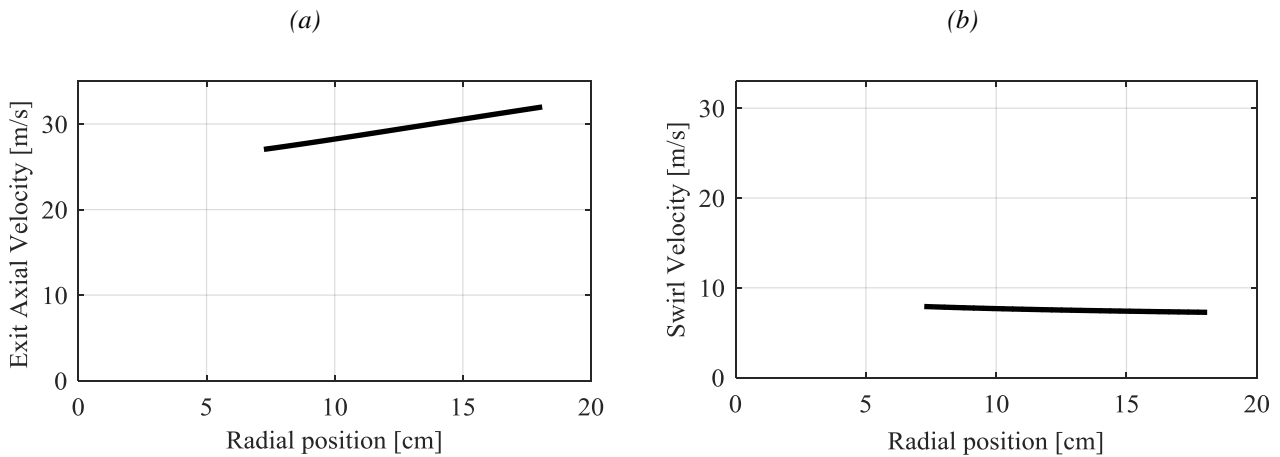


Figure 1: Optimum (a) exit axial velocity and (b) swirl velocity profile.

### Control Vortex Fan Design

An axial fan with a diameter of 0.362 meters (14.25 inches) has been designed using the CVD method to generate the axial velocity profile and swirl velocity shown in Figure 1. Using an E214-airfoil (Selig et al., 1989) the blade twist and chord distribution to generate the desired axial velocity and swirl velocity profile where determined for a fan with 11 blades and a hub to tip ratio of 0.4. The resulting chord and twist distribution for the fan blade sections is shown in Figure 2. As illustrated in Figure 2(a) the chord distribution increases slightly from the hub to the tip. The resulting fan geometry is shown in in Figure 3. The fan volumetric flow rate and mechanical power for a range of fan speeds from 0 to 3000 RPM is shown in Figure 4. Here, it can also be illustrated that the design volumetric flow rate is 5559 CFM at the design fan speed of 2500 RPM (tip Mach number of 0.14). The corresponding mechanical power is 1820 watts. The fan predicted overall A-weighted sound power level for a range of fan speeds from 0 to 3000 RPM is shown in Figure 5. The estimated overall sound power level at the design fan speed of 2500 RPM is 70 dB(A).

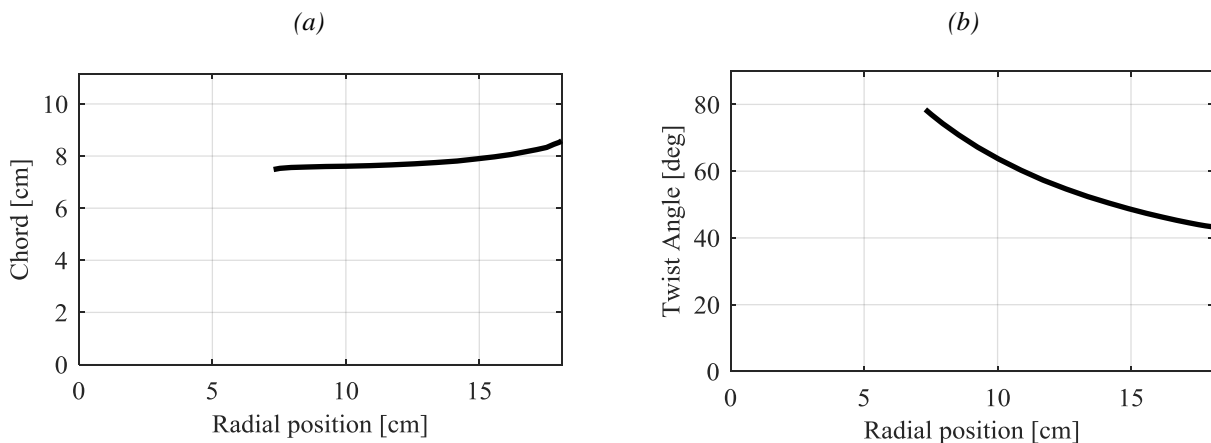


Figure 2: Fan design (a) chord, and (b) twist geometry.

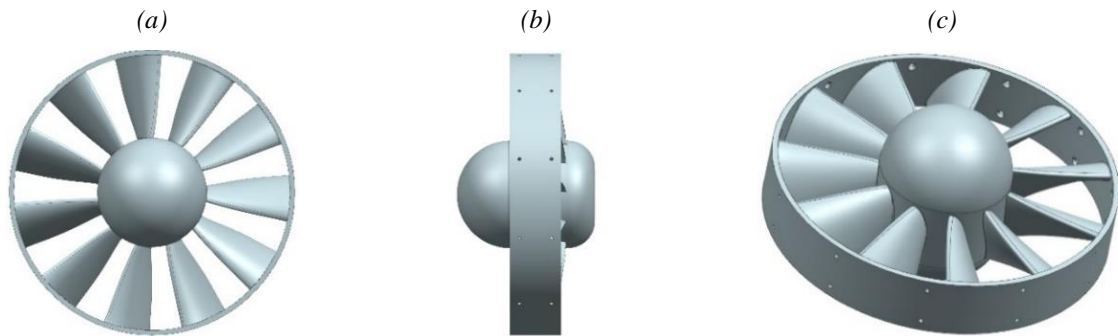


Figure 3: Control vortex fan design: (a) front view, (b) side view, and (c) isometric view.

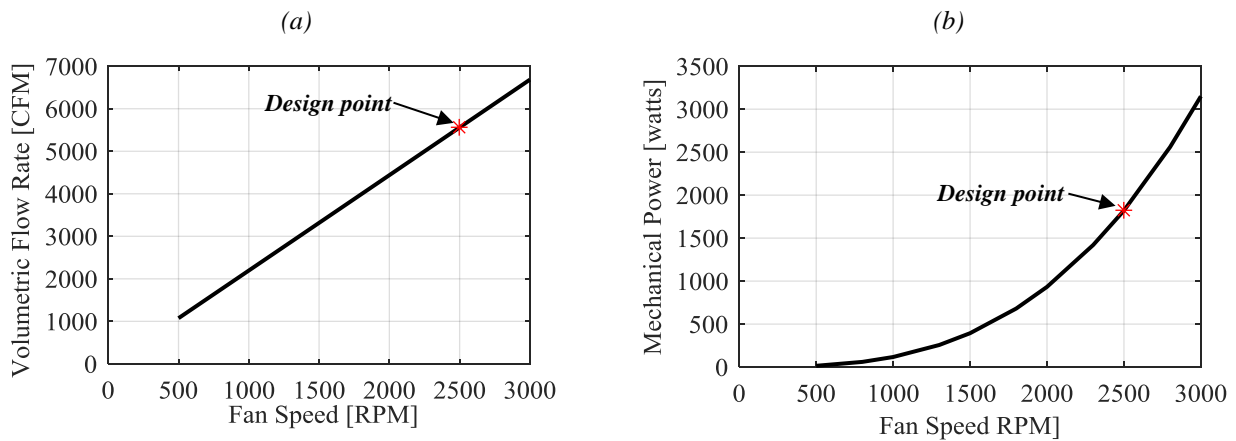


Figure 4: Control vortex fan performance: (a) volumetric flow rate and (b) mechanical power vs fan speed.

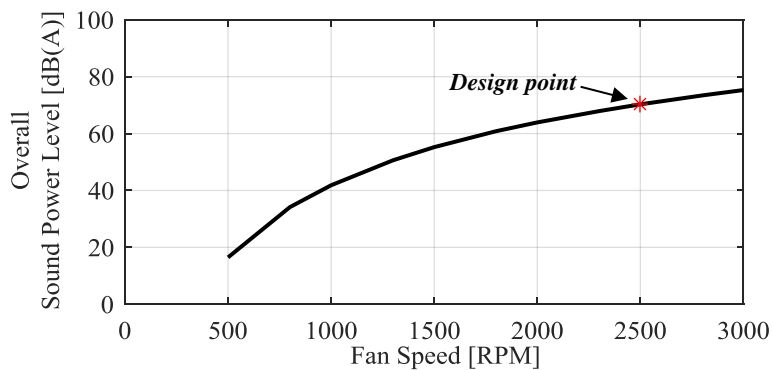


Figure 5: Control vortex fan noise overall sound power level vs fan speed.

### Inlet duct design

To properly direct the upstream flow so that the flow is uniform in front plane of the fan, a bell mouth inlet duct was designed. The design of the inlet and rear ducts was conducted using DFDC. As part of the design process, a trade study was conducted to identify the duct geometry that will result in a uniform inlet flow while increasing the fan performance. The trade study was carried out by changing parameters of the elliptical bell mouth inlet with a fixed cylindrical rear duct outlet. The final inlet bell mouth duct has a diameter of 0.58 m or 1.32 times the fan

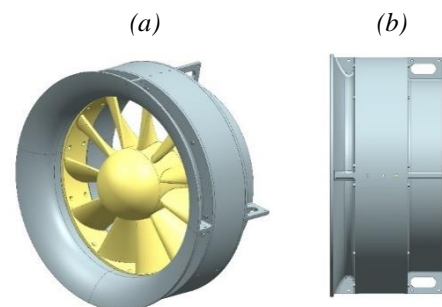


Figure 6: Duct geometry (a) isometric view, and (b) side view.

diameter. The static thrust increase due to the duct design resulted in a volumetric flow rate rise of approximately 8%. The final duct geometry is shown in Figure 6. The resulting velocity profile with the designed duct geometry is compared to the design velocity profile. Additionally, the DFDC velocity profile is adjusted to account for the duct boundary layer. The boundary layer profile was estimated using the 1/7<sup>th</sup> power law profile for turbulent flow in a smooth cylinder (Sawchuk and Zamir, 1992) described as

$$u(y) = \left(\frac{y}{\delta}\right)^{1/7} U_{edg} \quad (8)$$

Where  $U_{edg}$  is the edge velocity and  $\delta$  is the boundary layer thickness, both estimated using DFDC. The resulting velocity profile as compared to XROTOR predictions is shown in Figure 7. It is important to note here that the differences between the XROTOR and the DFDC profile is that the effect of the duct is included in the later one. In addition, the effect of the boundary layer is also accounted for in DFDC.

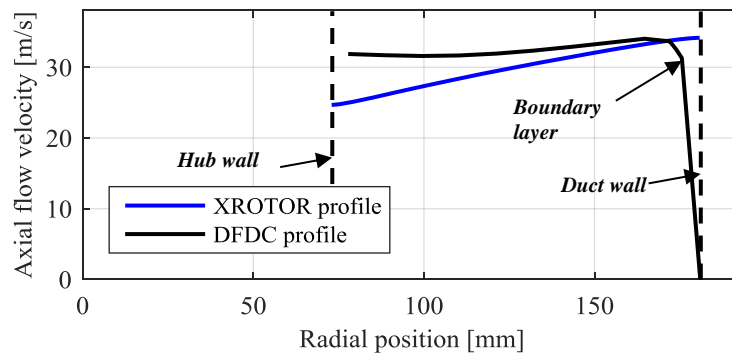


Figure 7: XROTOR CVD fan design velocity profile comparison to the DFDC CVD ducted fan velocity profile.

## EXPERIMENTAL TEST

The fan and duct were fabricated using an Objet500 Connex3 and Fortus 450mc 3D printer respectively. The CVD fan was 3D printed using the RGD525 material with an accuracy up to 200 microns ( $10^{-6}$  m). The RGD525 has a high dimensional stability and tensile strength of 70-80 MPa (10,000-11,500 psi) which resulted in a smooth finish. The duct design was 3D printed using the ABS Plus material with an accuracy of  $\pm .127$  mm. The CVD fan and duct prototype is shown in Figure 8. Testing of the CVD fan prototype was conducted in the anechoic chamber (cutoff frequency of 100 Hz) at Virginia Tech with dimensions of 5.4x4.1x2.4 m from wedge tips to wedge tips. The main noise instrumentation was a 2.8 m diameter far-field arc array. The far field arc is composed of 19 microphones evenly distributed along its circumference, i.e. from 0 to 180 degrees. The experimental set up is shown in Figure 8. The flow measurements and fan speed were directly measured using a pitot-static tube and optical sensor respectively. A linear traverse system was used to traverse the pitot static tube across the fan radius. The electrical power was measured indirectly using the motor controller sensor.

As shown in Figure 8, the prototype fan was tested in two configurations: a rim-mounted and a hub mounted or free-tip. The rim mounted design was built and implemented using three bearing mechanisms to support the fan. The bearing mechanism houses 2 miniature high speed bearings slightly pressed fitted in a cylinder. Then, O-rings are slid into the housing to minimize metal to metal noise from the direct contact of the miniature bearing and the aluminum ring attached to the fan. The free-tip configuration is the more conventional shaft mounted fan with no rim support.

The motor used to drive the fan in both configurations is the ThinGap TG7140 with a maximum torque of 4.52 N·m and a maximum speed of 8141 RPM. Since the fan nominal torque is 6.95 N·m

at a nominal fan speed of 2500 RPM, the ThinGap TG7140 is not able to provide enough torque to run the fan. Thus, a gearbox with a ratio of 3 is used such that the ThinGap motor provides a maximum torque of 13.52 N·m at a maximum speed of 2713 RPM. Consequently, a gearbox was added as illustrated in Figure 8.

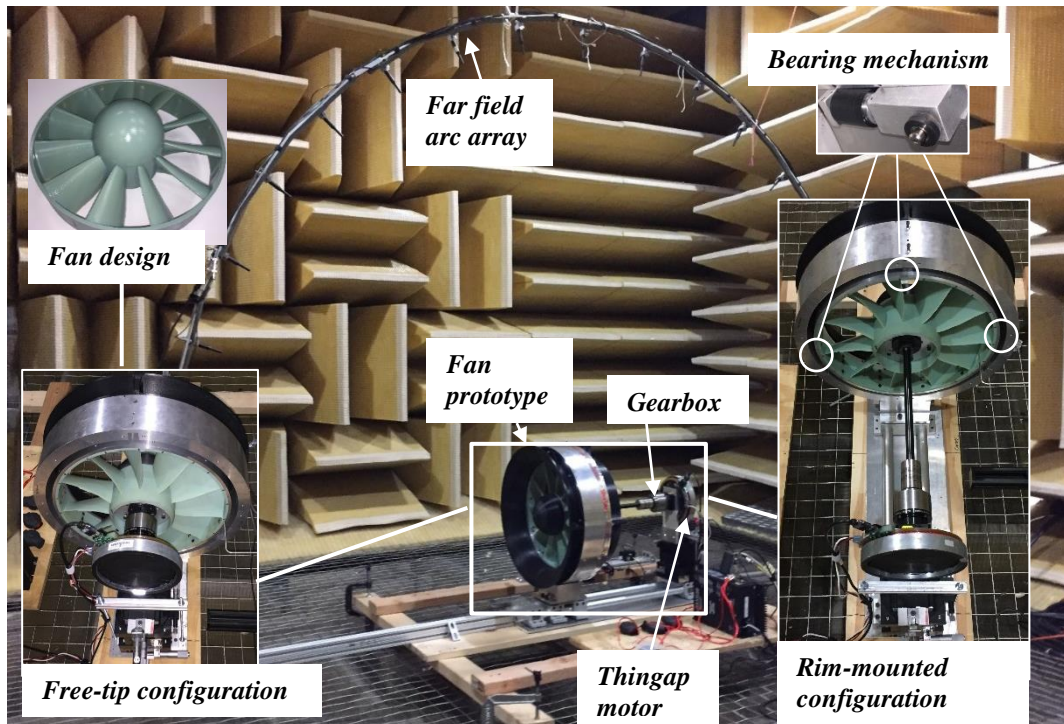


Figure 8: Noise measurements experimental set-up.

## Experimental results

This section presents key results from testing the fan for both configurations shown in Figure 8. The free-tip and rim-mounted approaches are compared using experimental results for the exit axial velocity profile, electric power, and fan noise. Additionally, the flow and mechanical power results are also compared to predictions from XROTOR and DFDC.

### Axial flow results

The aerodynamic characteristic of the fan under both configurations was determined by measuring the velocity profile along the radius of the fan at a fixed fan speed. Figure 9(a) shows the measured velocity profile for the rim mounted and the free tip configurations as compared to the DFDC predictions at a fan speed of 1000 RPM. As illustrated here, the rim-mounted approach shows good agreement with DFDC up to  $2/3^{\text{rd}}$  of the blade span. Since the fan speed here is 40% of the design speed, the viscous effects are dominant near the wall, i.e. large boundary layer. It is also evident from Figure 8 that blockage in the free-tip approach resulted in lower axial velocities near the hub with a slight increase near the fan blade tip. The velocity profile for CVD under the free-tip configuration is compare to DFDC in Figure 9(b) for a fan speed of 1600 RPM, i.e. 64 % of the design speed. As shown, the fan exit axial velocity is under predicted for half of the blade span with an over prediction near the hub wall due to the blockage of the free-tip configuration. However, good agreement between the DFDC prediction and measured velocity profile is observed near the wall. Additionally, Figure 10 shows the volumetric flow rate of the fan measured at different fan

speeds (free-tip configuration). As illustrated, volumetric flow rate measured at all fan speeds is in good agreement with predictions, i.e. within 10 % of the predicted volumetric flow rate.

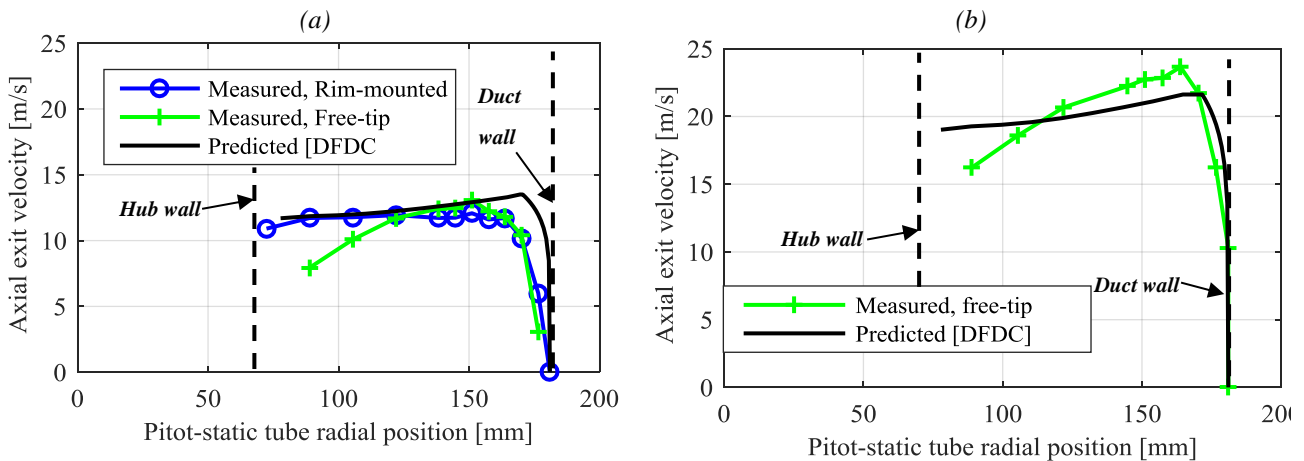


Figure 9: Velocity profile for free-tip ducted fan comparison to DFDC predictions for fan speed of (a) 1000 RPM, and (b) 1600 RPM.

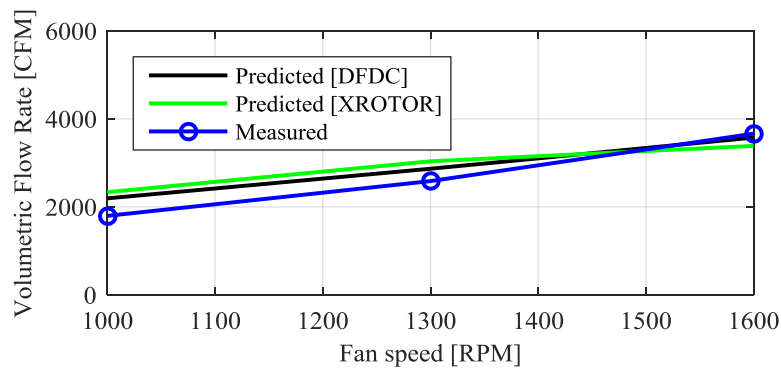


Figure 10: Fan volumetric flow rate vs fan speed for free-tip configuration.

### Power results

The power consumption of the fan was carried out to validate the design and to compare the free-tip to the rim-mounted configuration. To this end, the measured mechanical power consumption of the fan is first compared to predictions from XROTOR in Figure 11. As illustrated here, the measurements and predictions agree very well indicating that the flow behaves well as expected, i.e. there is no stall. Furthermore, the electrical power consumption of the free-tip configuration is compared to the rim-mounted configuration in Figure 12. As shown here, the power consumption of the rim-mounted approach is approximately 80% higher than the free-tip configuration. The major source of power consumption is the rolling resistance introduced by the O-rings used to minimize metal to metal noise from the direct contact of the bearing and the aluminum ring. These O-rings introduced excessive mechanical losses that made this implementation not practical (losses are due to deformation of the viscoelastic O-rings). The losses in these O-rings were more than the aerodynamic mechanical power required to operate the fan. For this reason, it is unlikely that the rim mounted approach is a practical approach unless this problem is overcome.

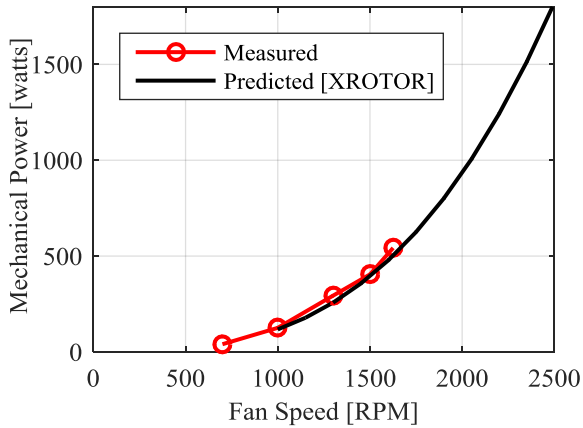


Figure 11: CVD Fan measured mechanical power comparison to XROTOR prediction.

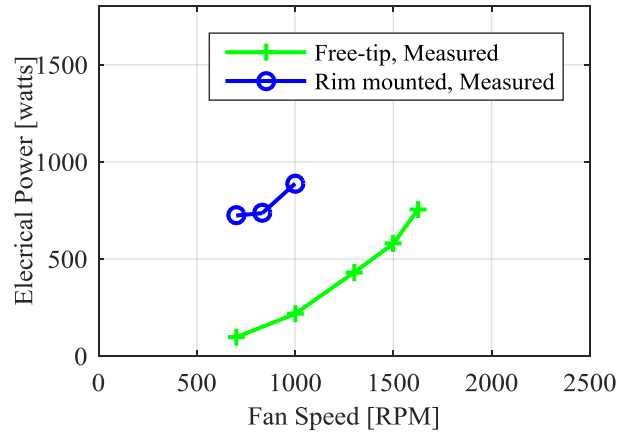


Figure 12: Rim mounted and free-tip electrical power comparison.

### Noise results

Noise measurements for the fan for both configurations were made using the far field arc array set up shown in Figure 8. The data was post processed to give the sound power level spectrum. The fan sound power level spectrum in 1/3<sup>rd</sup> octave bands for fan speeds of 1000 RPM and 1600 RPM are shown in Figure 13 and Figure 14, respectively. Although the rim mounted approach eliminates dominant sources of aerodynamic noise, it does introduce significant noise due to vibration of the duct, e.g. vibration induced by fan propagates through the 3 bearings and excites the duct. As shown in Figure 13, the rim mounted approach increased noise levels by 8 dB relative to the free tip configuration. Consequently, it has been determined that the rim-mounted approach is not practical. The sound power level in 1/3<sup>rd</sup> octave bands in Figure 14 shows that the overall sound power level of the free tip fan at a speed of 1600 RPM is 77.8 dB(A).

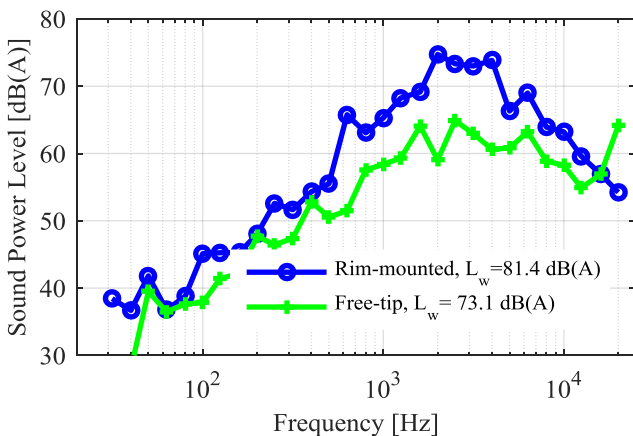


Figure 13: Sound power level at 1000 RPM for the rim-mounted and free tip configurations.

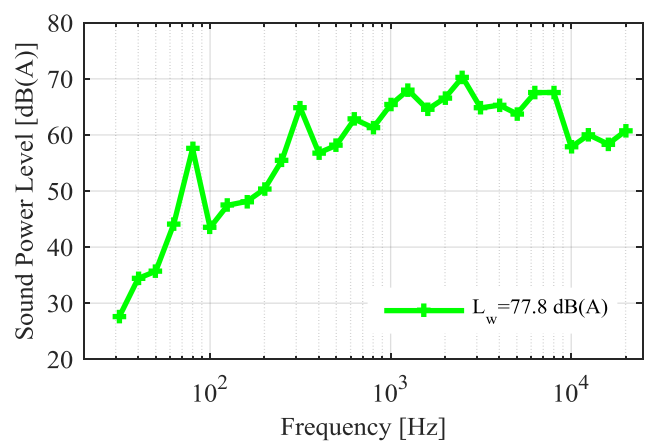


Figure 14: Sound power level at 1600 RPM for the free tip configuration.

To gain more insight into the test rig noise characteristics, the narrow band sound power level spectrum for the free-tip configuration at two fan speeds is shown in Figure 15. As illustrated, the noise measurements made include both fan and motor noise with motor noise dominating at higher frequencies. As illustrated, the fan noise scales with the 4-6<sup>th</sup> power of the fan speed for frequencies lower than 2000 Hz. However, the sound power level spectrum is relatively the same for frequencies higher than 2500 Hz. This is evidence that the Free-tip fan noise is dominated by the

electric motor noise at higher frequencies. Consequently, to further reduce the noise of the fan prototype, the motor noise must be reduced.

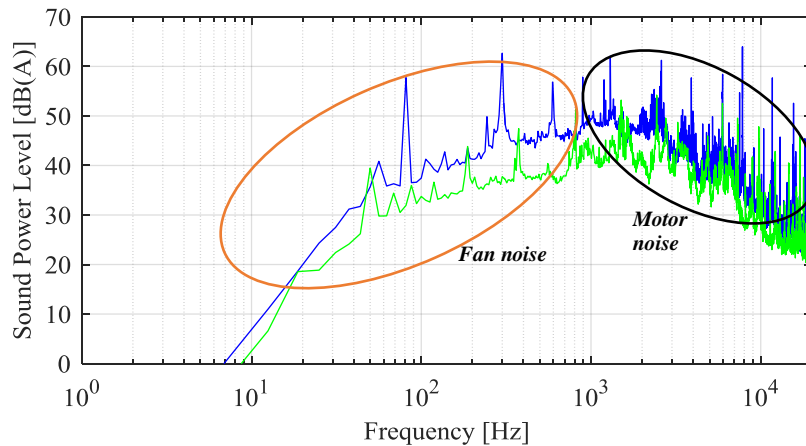


Figure 15: Fan sound power level spectrum at two fan speeds.

### Comparison to commercial ventilation fans

Since noise is proportional to the 4-6<sup>th</sup> power of the fan speed, the fan noise is significantly reduced by reducing the fan speed. To this end, the trend in the design of fans has been to reduce the fan speed while increasing the fan diameter to maintain the volumetric flow rate. However, floor space restrictions in working areas can significantly impact the fan selection. Consequently, a compact fan can free up valuable work space while maintaining a safe work environment (Lawrence Berkeley National Laboratory, 1989). Hence, the approach here has been to lower the fan tip speed while maintaining the aerodynamic performance and restricting the size of the fan diameter. This approach requires designing the fan blades to increase the contribution of the fan blade outer sections. This resulted in a compact, low tip speed fan with a high volumetric flow rate. In Figure 16 the sound power level is plotted as a function of the volumetric flow rate for a large number of commercial ventilation fans. The sound power level and CFM for these commercial fans were obtained from published manufactured data, e.g. data was assumed accurate. The results for the fan designed in this work is also included and labeled CVD fan. As shown in the figure, the CVD fan at the measured fan speed (64% of the design fan speed) outperforms in terms of noise and/or CFM most of the commercial fans. The few commercial fans that are quieter and generate more CFM than the CVD fan are inside the shaded area in the plot. The fan diameter for these fans is also indicated in the figure. It is noticeable that all of these fans have diameters that are between 25% and 100% larger than the CVD fan, i.e. 0.45 to 0.71 m versus 0.362 m for the CVD fan. Additionally, it is important to note here that at the fan design speed, the CVD fan is expected to generate a volumetric flow rate of 6000 CFM with a fan sound power level of 70 dB(A) as shown in Figure 16, e.g. electric motor noise not included in this estimate. Although not experimentally verified due to motor power limitations, it helps illustrate the capability of the CVD fan.

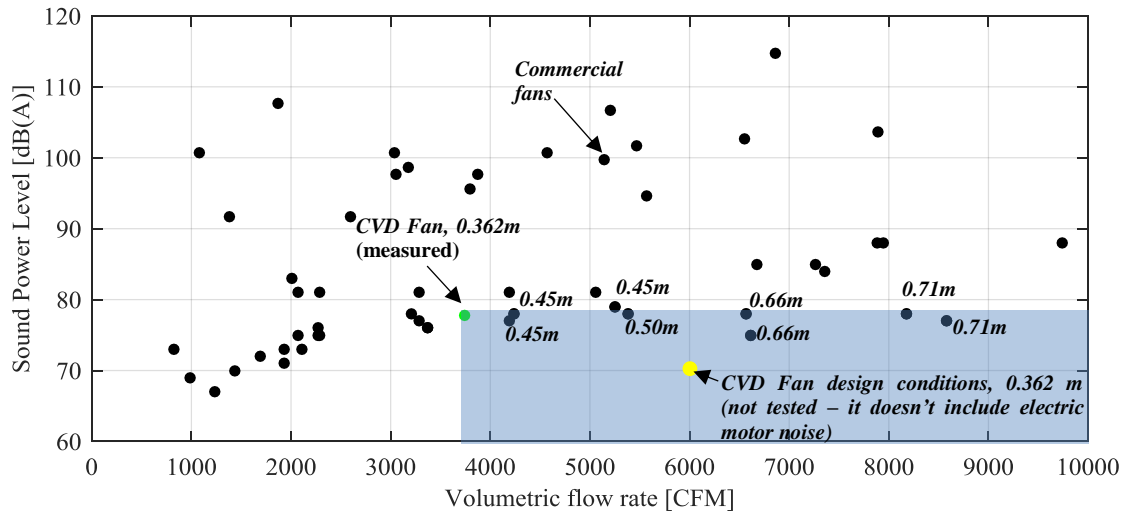


Figure 16: CVD fan comparison to commercial ventilation fans.

## CONCLUSION

The design of a quiet axial fan has been accomplished using a control vortex fan design approach. The key approach to reduce noise was to reduce the tip speed as much as possible while maintaining aerodynamic performance. The blade sections have been designed to generate an axial and swirl velocity distribution that results in radial equilibrium and in lower exit dynamic losses. The fan has been fabricated using 3D printed technology. The fan was tested in two configurations: a rim-mounted and hub mounted (free-tip). Results show that the rim mounted approach introduces significant mechanical losses and noise that make the concept impractical with the current technology. Furthermore, the free-tip test was used to measure the fan aerodynamic performance and power consumptions showing excellent agreement with predictions. Additionally, the measured fan aerodynamic performance and noise were compared to a large number of commercial ventilation fans showing that the CVD fan outperforms most commercial fans with a smaller fan diameter. The fans that outperform the CVD fan in terms of sound power level and volumetric flow rate have diameters that are between 25% and 100% larger than the CVD fan. Consequently, it has been shown that it is possible to maintain the volumetric flow rate by better design of the fan blades instead of simply increasing the fan diameter. Therefore, it is possible to design small compact fans that are easily implemented in the workplace while maintaining the same volumetric flow rate and reducing noise levels.

## ACKNOWLEDGEMENTS

This study was sponsored by the Alpha Foundation (Award Number: AFC215-21) for the Improvement of Mine Safety and Health. The views, opinions and recommendations expressed herein are solely those of the authors and do not imply any endorsement by the Alpha Foundation, its Directors and staff.

## BIBLIOGRAPHY

- [1] Padhy, S. K. – *Noise generation in small axial flow fans: analysis and some design guidelines for noise reduction*. Paper presented at the 45th Annual International Appliance Technical Conference Designs on Technology, 9-11 May 1994, Madison, WI, USA, **1994**
- [2] Cudina, M. – *Noise generated by a vane-axial fan with inlet guide vanes*. *Noise Control Engineering Journal*, 39(1), 21-30, **1992**
- [3] Bruneau, P. R. P. – *The design of a single rotor axial flow fan for a cooling tower application*. Stellenbosch: University of Stellenbosch, **1994**
- [4] Davis, D. G. M. – *The impact of noise regulations on propeller design*, **1979**
- [5] Vad, J., Bencze, F. – *Three-dimensional flow in axial flow fans of non-free vortex design*. *International Journal of Heat and Fluid Flow*, 19(6), 601-607, **1998**
- [6] Drela, M., Youngren, H., – *XROTOR*, Cambridge, MA: Massachusetts Institute of Technology. Retrieved from <http://web.mit.edu/drela/Public/web/xrotor/>, **2005**
- [7] Drela, M., Youngren, H., – *Ducted Fan Design Code (DFDC)*, Cambridge, MA: Massachusetts Institute of Technology. Retrieved from <http://web.mit.edu/drela/Public/web/dfdc/>, **2011**
- [8] Mugridge, B. D., Morfey, C. L., – *Sources of noise in axial flow fans*. *Journal of the Acoustical Society of America*, 51(5), 1411-1427, **1972**
- [9] Parzych, H. a., – *Theory for noise of propellers in angular inflow with parametric studies and experimental verification*. Retrieved from <https://ntrs.nasa.gov/search.jsp?R=19930015905>, **1993**
- [10] Vad, J., Horváth, C. – *The impact of the vortex design method on the stall behavior of axial flow fan and compressor rotors*. Paper presented at the 2008 ASME Turbo Expo, June 9, 2008 - June 13, 2008, Berlin, Germany, **2008**
- [11] Dixon, S. L., Hall, C. – *Fluid Mechanics and Thermodynamics of Turbomachinery: Seventh Edition*, Elsevier Inc., **2013**
- [12] Hurtado, M. P., Wu, D., Burdisso, R. – *Design of Low Speed Rim Driven Ventilation Fan for Minimum Noise*. Paper presented at the NOISE-CON2017, Grand Rapids, Michigan, **2017**
- [13] Von Backström, T. W., Buys, J. D., Stinnes, W. H. – *Minimization of the exit loss of a rotor-only axial fan*. *Engineering Optimization*, 26(1), 25-33, **1996**
- [14] Selig, M. S., Donovan, J. F., Fraser, D. B. – *Airfoils at low speeds*. Retrieved from Virginia Beach, Virginia, **1989**
- [15] Sawchuk, S. P., Zamir, M. *Boundary layer on a circular cylinder in axial flow*. *International Journal of Heat and Fluid Flow*, 13(2), 184-188. **1992**
- [16] Lawrence Berkeley National Laboratory – *Improving Fan System Performance, a source for industry*. The United States Department of Energy and Air Movement and Control Association International, Inc. **1989**